Highly Transparent and Conductive Electrodes Enabled by Scalable Printing-and-Sintering of Silver Nanowires

Weiwei Li,*[1] Emre Yarali,[2] Azamat Bakytbekov,[1] Thomas D. Anthopoulos[2] and Atif Shamim[1]

[1]IMPACT Lab, Computer, Electrical and Mathematical Sciences and Engineering (CEMSE) Division, King Abdullah University of Science and Technology (KAUST), Thuwal 23955-6900, Kingdom of Saudi Arabia

[2]KAUST Solar Center, King Abdullah University of Science and Technology (KAUST), Thuwal 23955-6900, Kingdom of Saudi Arabia

E-mail: weiwei.li@kaust.edu.sa

Abstract. Silver nanowires (Ag NWs) have promised well for flexible and transparent electronics. However, It remains an open question on how to achieve large-scale printing of Ag NWs with high optical transparency, electrical conductivity, and mechanical durability for practical applications, though extensive research for more than one decade. In this work, we propose a possible solution that integrates screen printing of Ag NWs with flash-light sintering (FLS). We demonstrate that the use of low-concentration, screen-printable Ag NW ink enables large-area and high-resolution patterning of Ag NWs. A critical advantage comes from the FLS process that allows low-temperature processing, short operational time, and high output rate – characteristics that fit the scalable manufacturing. Importantly, we show that the resultant Ag NW patterns feature low sheet resistance (1.1-9.2 Ohm/sq), high transparency (75.2-92.6%), and thus a remarkable figure of merit comparable to state of the art. These outstanding properties of Ag NW patterns, together with their scalable fabrication method we proposed, would facilitate many Ag NW-based

applications, such as transparent heater, stretchable displays, and wearable devices; here, we demonstrate the novel design of flexible and transparent radio frequency 5G antennas.

Keywords: Screen Printing, Silver Nanowires, Flash Light Sintering, Transparent Electronics

Introduction

With the recent interest in optically transparent electronics, transparent conductive electrodes have been extensively studied[1, 9, 16, 49, 50, 60]. In particular, various emerging nanomaterials, including conductive polymers[61], carbon materials (carbon nanotube[23], graphene[42]), metal nanowires[7, 12, 45], and metal mesh[30, 51], have been leveraged for the development of electrodes with high transparency and conductivity. Among these materials, silver nanowires (Ag NWs) are quite promising as many reports revealed that the Ag NWs could achieve thin films with sheet resistance and optical transmittance comparable to conventional transparent metal oxides[33, 46]. Another mechanical advantage of Ag NWs is their mechanical flexibility that may maintain electrical conductivity even under external deformation[15, 24, 25].

A number of issues need to be addressed before Ag NWs can truly contribute to transparent electronics. One is to pattern Ag NWs in deterministic shapes and sizes. A variety of techniques have been utilized to pattern the Ag NWs, such as photolithography[48, 51], shadow masking[5, 54], ultraviolet ozone surface treatment[27, 58], and dry transfer process[38]. However, these techniques either require multiple processing steps or suffer from limited patterning size that also limits the patterning efficiency. One-step printing seems to be an alternative method that allows efficient, scalable manufacturing. However, inkjet printing of Ag NWs requires short nanowires that can pass through the nozzles without clogging; Screen-printable and gravure-printable inks need either high Ag NWs loading[2, 19, 37, 55] or added insulating

binders[14]. As a consequence, the printed electrodes typically compromise in functional performances, including low conductivity (<10^6 S/m)[18],[10] and poor optical transparency (<75%)[3, 14, 35]. It, therefore, remains an open question on how to achieve large-scale printing of Ag NWs with high optical transparency, electrical conductivity, and mechanical durability for practical applications, though extensive research efforts in this area.

In this work, we developed a custom Ag NWs ink suitable for screen printing. With the help of screen printing and xenon flash-light sintering (FLS), we fabricated large-area electrodes with high conductivity and optical transparency simultaneously. The screen-printable Ag NW ink with low Ag loading (about 0.9 wt.%) is developed by introducing polyvinyl pyrrolidone (PVP) with ultrahigh molecular weight (Mw = 2 × 10^6 - 3 × 10^6 g/mol) as a binder material, which is beneficial to highly transparent patterns. The ink composition is optimized to allow the deposition of Ag NW patterns with a good spatial resolution (approximately 50 μm for line width and line spacing). Then, FLS is utilized to sinter the printed Ag NW patterns in milliseconds, enabling more than 70% enhancement of electrical conductivity (as compared to non-sintered electrodes) without any degradation in the optical transparency. We obtain scalable Ag NW patterns with extremely low sheet resistance (1.1-9.2 Ohm/sq), ultrahigh transparency (75.2-92.6% in transmittance), and superior figure of merit (FoM, more than 1100). Moreover, the printed and flash-sintered Ag NW patterns demonstrate outstanding mechanical flexibility, showing negligible changes in resistance after 1000 bending cycles. These features fit flexible, transparent, and high-performance electronic devices. As a proof of concept, we demonstrate a multi-frequency radio frequency (RF) antenna, capable of working in the WiFi, Bluetooth, and 5G bands.

Experimental Section

Raw Materials

Silver nitrate ($AgNO_3$), ethylene glycol (EG), iron (III) chloride ($FeCl_3$), polyvinyl pyrrolidone (PVP, M_w: 55,000, 1,300,000), propylene glycol, isopropanol and 2-butoxyethanol are purchased from Sigma-Aldrich. PVP (K120) is obtained from Ashland.

Synthesis of Ag NWs

The Ag NWs are synthesized through a modified polyol process. Briefly, PVP (M_w=55,000, 0.85 g, M_w=360,000, 0.85 g) are added to EG (200 mL) with stirring. Next, $AgNO_3$ (2 g) is added to the PVP solution. After complete dissolution, $FeCl_3$ solution (28 g, 0.6 mM in EG) is added and stirred for 2 minutes. Then, the mixture is transferred to a preheated round-bottom flask at 130 °C and allowed reaction for 4 h. After cooling to room temperature, the Ag NWs are washed using acetone and ethanol for 3 cycles.

Formulation of Ag NWs-Based Screen-Printable Ink

The ink is formulated by mixing the washed Ag NWs with PVP solution. First, 3 g of PVP (K120, M_w=2 × 10^6 - 3 × 10^6 g/mol) is dissolved in a solvent mixture containing of propylene glycol, isopropanol and 2-butoxyethanol with a ratio of 8:1:1. Then, Ag NWs are mixed with PVP solution and agitated thoroughly using a propeller stirrer at a speed of 1500 rpm for 20 min to obtain the Ag NW ink.

Screen Printing of Ag NWs

The Ag NWs patterns and antennas are printed on clean PET substrates using a screen stencil with a mesh count of 325, a wire diameter of 20 µm, and an emulsion thickness of 10 µm. Next, the printed samples are dried at 80 °C for 10 min in an oven to evaporate solvents. Then, the Ag NW samples are immersed in warm water (60 °C) or ethanol for 5 min to remove most of the PVP (k120), while remaining the Ag NWs at the original position.

Flash Light Sintering

Flash light sintering is conducted using Novacentrix Pulse Forge 1300 system. During processing, the distance between the sample and flash lamp is kept at 5 mm. The pulse length, pulse voltage and pulse number are optimized as given in the text.

Antenna simulation

High Frequency Structure Simulator (HFSS) is utilized to perform the simulation for the fractal antenna. A 3D model, containing two conductor layers and a dielectric layer, is constructed. The dielectric substrate has a dielectric constant of 2.36, a dielectric loss tangent of 0.005 at 1 GHz, and a thickness of 0.1 mm. The conductor has an electrical conductivity of 5×10^6 S/m and a thickness of 1 μm. A discrete 50-ohm port is molded as the source.

Characterization

The morphologies of Ag NWs are characterized by SEM (ZEISS Merlin). The structure of Ag NWs is characterized by XRD (Bruker D2 PHASER). Thermal gravimetric analysis is performed using a TG 209 F1. The rheological behaviour of the formulated Ag NW ink is tested using an AR1500 rheometer (TA Instruments). The sheet resistance of the Ag NW patterns is measured using a four-probe resistance tester (CMT-SR2000N). The transparency is evaluated using a UV-Visible Spectroscopy (Thermo Evolution 600). The thickness of the Ag NW film is measured using a surface profiler (Veeco Dektak 150). RF measurements are performed using an Aglient N5225A Vector Network Analyzer. The S-parameters of the antennas are acquired from 1 to 6 GHz after RF calibration conducted based on the short-open-load (SOL) method to eliminate parasitic effects of the measurement system. The antenna gain and radiation pattern of the antenna are obtained in a tapered anechoic chamber (Satimo Starlab). Before measurement, the chamber is calibrated using NSI 2 - 18 GHz horn antenna.

Results and Discussion

To ensure a stable and high resolution (i.e. 50 µm) printing of Ag NWs, we introduce a viscous polymer matrix containing PVP and a solvent mixture (propylene glycol, isopropanol, and 2-butoxyethanol) to disperse high-aspect-ratio Ag NWs (length-to-diameter ratio > 600; Fig. S1) with low Ag loading (about 0.9 wt.%; Fig. S2a). The prepared Ag NW ink is stable, and no settlement of Ag NWs is observed after two months at 4 °C (Fig. S2b). A shear-thinning behaviour is observed in the rheological curve, and the ink had a viscosity of 4.7 Pa s at a shear rate of 1 s^{-1} (Fig. S2b). With this ink, desired patterns with high transparency are precisely deposited onto the target substrates at speed higher than 200 mm/s. When the printing process is complete, the printed Ag NW patterns are cured at 80 °C for 5 min to evaporate the solvents and obtain dry and dense Ag NWs films. Then, a warm water bath (60 °C) or ethanol bath, is used to help the Ag NW patterns recover their conductivity via PVP dissolving in the bath solution[19, 37], as can be observed in the SEM images of the Ag NWs before and after the bath in Fig. S3. Following the binder removal step, the conductive Ag NW patterns are exposed to pulsed flash-light to weld the NW junctions to further enhance the electrical conductivity.

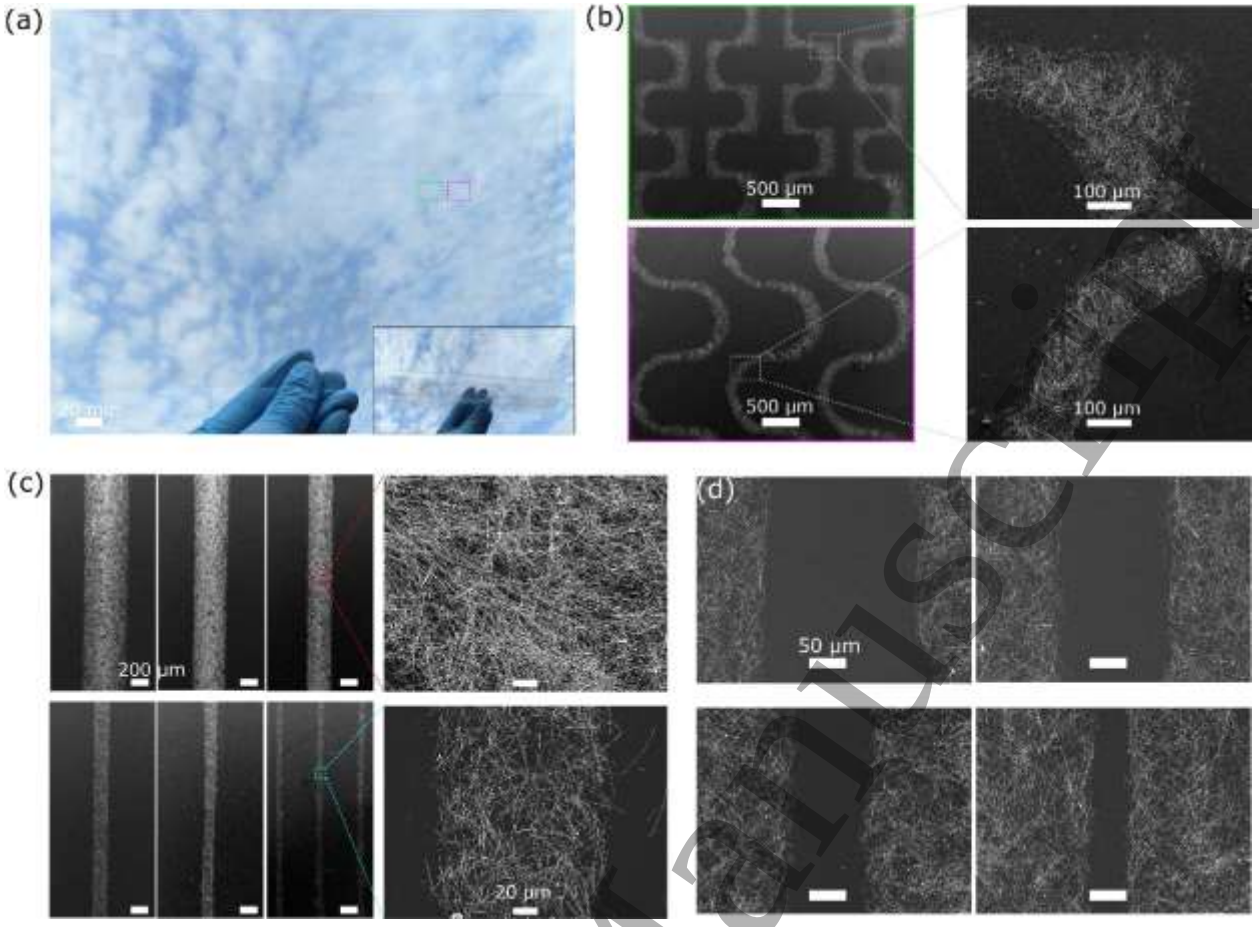

Fig. 1. Large-area and high-resolution printing of Ag NWs: (a) digital photograph of the screen-printed Ag NW patterns with an optical transmittance of 92% at λ = 550 nm on a PET substrate. (inset: the rolling status of the Ag NW patterns, demonstrating the flexibility); (b) SEM images of the screen-printed Ag NW serpentine line patterns and spiral line patterns (the right panel displays magnified SEM images of the edge of the Ag NW patterns); (c) SEM images of the screen-printed Ag NW lines with different line widths from 500 μm to 50 μm (the right panels present the Ag NW network and the edge of the Ag NW line); (d) SEM images of the screen-printed Ag NW patterns with different spacing of 200, 150, 100, and 50 μm.

The developed Ag NW ink and the screen-printing technique enabled one-step, direct patterning of Ag NWs in a large area and in high resolution. Fig. 1a and Fig. S4 present digital photographs of the printed Ag NWs patterns with different transparency (transmittance at λ=500 nm: from 92% to 82% and 75%) on flexible polyethylene terephthalate (PET) substrates with a dimension of 200 × 200 mm^2, and on a rigid glass substrate with a diameter of 100 mm. From the scanning electron microscope (SEM) images in Fig.

1b, we found the precise, sharp, and smooth edges of the screen-printed Ag NW patterns. In addition, printed Ag NW lines with various line width are achieved successfully, and the narrowest is approximately 50 μm, as shown in the SEM images in Fig. 1c. Note that, line width of about 50 μm is close to the limit for screen-printing technique due to the resolution of the screen, and this has been confirmed by many other reports in the literature[20, 37]. In addition to the printed fine lines, different line spacing is attained. As displayed in Fig. 1d, all the printed spacing are in uniform shapes and smooth edges, and the printed spacing are 206(±10), 153(±6), 102(±9), and 48(±5) μm.

The morphological features of the pristine and the flash-sintered Ag NWs are investigated via SEM. As Fig. S5a depicts, the pristine NWs have loose contact points with a gap between the NWs, resulting in high electrical resistance[40]. However, the flash-sintered Ag NWs demonstrate strong welded junctions, and the gaps between NWs become smaller and even disappear, as Fig. 2a, 2b and Fig. S5b illustrate. The welded junctions decrease the resistance of the Ag NWs patterns and hence improve the electrical conductivity.

When placed under the flash lamp at a distance of 5 mm, the Ag NWs are exposed and illuminated by a high-intensity pulsed light with a broad wavelength of 200–1500 nm. It is believed that such illumination will generate highly localized heating only at the NW junctions[6, 29, 44]. This phenomenon, also known as “hot spot”, can result in the welding of the Ag NW junctions because of the high-temperature thermal process. To further understand the effect of the FLS on lowering the resistance of the screen-printed Ag NW patterns, we study various parameters of the sintering process, including pulse length, pulse voltage, energy density (which depends on the pulse length and applied voltage) and pulse number. We choose Ag NW patterns with an initial sheet resistance of approximately 46 ohm/sq and a transmittance of 91.6 % at λ = 550 nm as a reference sample. First, the sample is sintered with different pulse lengths (corresponding to different energy densities), keeping the same pulse voltage of 350 V and pulse number of 40. The measured sheet resistances decrease almost linearly from 46 ohm/sq to 11 ohm/sq as the pulse length

increases from 100 μs to 600 μs (corresponding to 0.93 J/cm^2, Fig. 2c). Then, the resistance remains nearly constant (about 10.3 ohm/sq) when the pulse length is further increased to 900 μs in which energy density corresponds to 1.385 J/cm^2, indicating the self-limiting behaviour of the inter-NW junctions. As expected, the transmittances of the Ag NW electrodes remain nearly constant (about 91.5%) during the flash sintering process even when exposed to high light energy density of 1.385 J/cm^2[6, 53]. Next, as the pulse voltage increases from 100 to 350 V using 50 V step (pulse length: 600 μs, pulse number: 40), the sheet resistances decrease from 45.9 ohm/sq to 10.1 ohm/sq (Fig. S6a) and reach a value of 10.3 ohm/sq for pulse voltages >400 V. Finally, when the sample is sintered for 40 pulses (24 ms total), the sheet resistance dramatically decreases from 46.6 ohm/sq to 9.6 ohm/sq (Fig. S6b). When further increasing the pulse numbers (over 50, corresponding to a exposure time of 30 ms), the sheet resistance only slightly increases to 10.4 ohm/sq[11]. To prove the effectiveness of the flash-sintering process, we print Ag NW patterns with various sheet resistance (5.8-42 ohm/sq) and transmittance (72-92.2%) via tuning the printing passes, and then sinter under FL with optimized parameters (pulse length: 600 μs; pulse voltage: 375 V, pulse number: 40). As presented in Fig. S7, the sheet resistances of all the screen-printed Ag NW patterns dramatically decrease by more than 70% (the maximum is 82.7%; Fig. S7) after exposure to FL for a total duration of 24 ms. To quantitatively demonstrate the superior electrical and optical performance of our screen-printed, flash-sintered Ag NW patterns and compare with the transparent electrodes in literature, we introduce the figure of merit (FoM) to define the trade-off between the electrical conductivity and optical transparency by considering the sheet resistance (R_s) and transmittance (T, at λ=550 nm) as expressed in Equation (1):

$$FoM = \frac{188.5}{R_s\left(T^{-1/2}-1\right)} \quad (1)$$

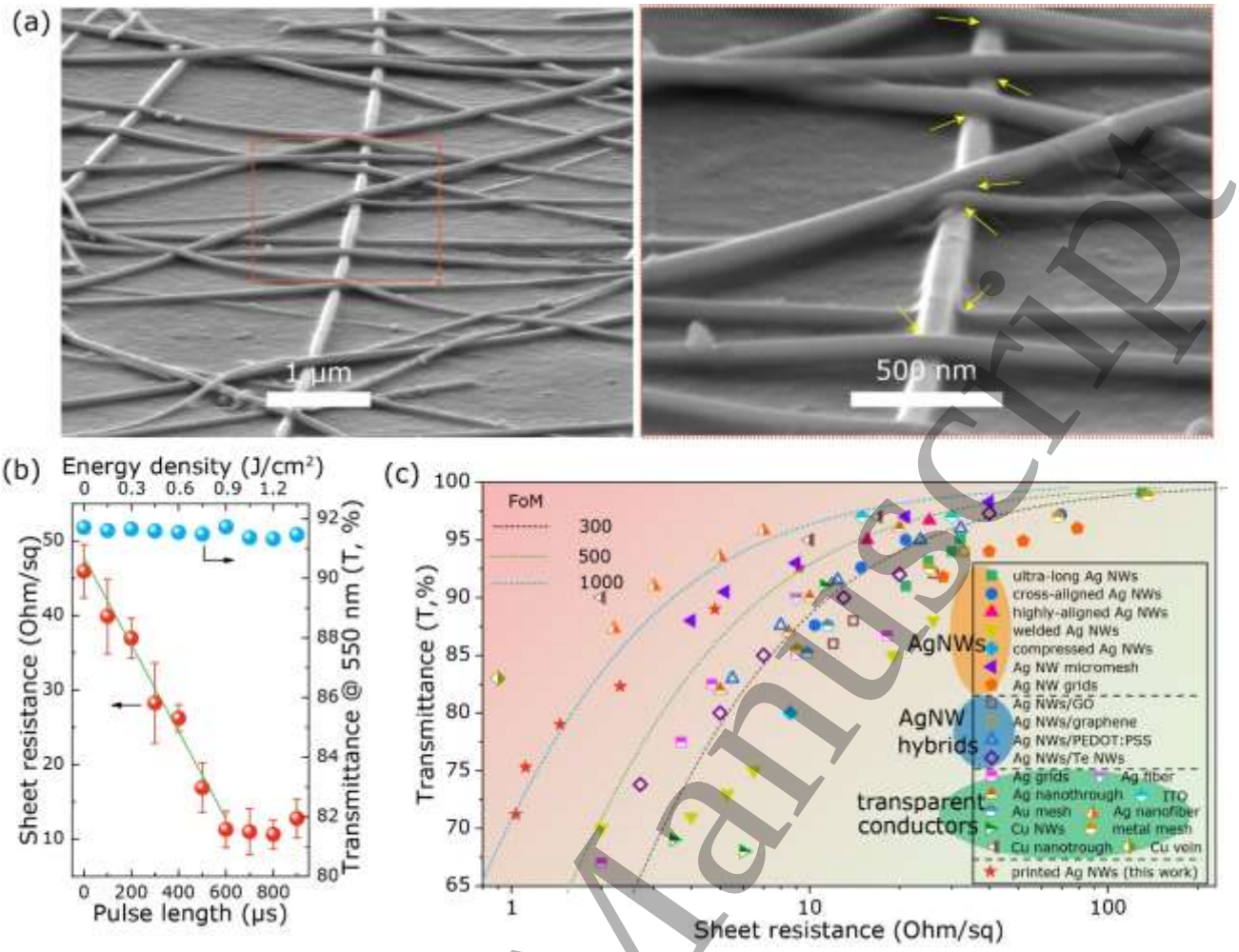

Fig. 2. (a) Tilted view SEM image of Ag NWs after the FLS process" The right panel is an enlarged SEM image in higher magnification, and the yellow arrows indicate the welded junctions between NWs; (b) the sheet resistance and optical transmittance at λ = 550 nm of the printed Ag NW patterns under different pulse lengths and energy densities of the flash light; (c) the sheet resistance versus optical transmittance (at λ = 550 nm) for the screen-printed, flash-sintered Ag NW patterns, along with some selected, important transparent electrodes reported in the literature (the dotted lines represent FoM of 300, 500, and 1000 according to Equation [1]).

Evidently, lower sheet resistance and higher transmittance values result in high FoM, which is highly desired for optoelectronic applications. Fig. 2c shows three fitted curves based on Equation (1) with FoM values of 300, 500, and 1000 (dashed lines). The transmittance of our screen-printed, flash-sintered Ag NW patterns with various sheet resistances are also indicated. All the FoM values are located on the left side of FoM = 300 at high transmittance (larger than 90%), indicating that the FoM values are over 300. In

comparison, most of the previously reported high-quality transparent conductive films exhibit FoM values below 300, with only some exceeding 500. Our printed Ag NW films exhibit the lowest sheet resistance with relatively high transmittance in comparison with values reported previously in the literature for Ag NWs-based[4, 26, 29, 33, 47, 51, 52] and Ag NW hybrid[31, 36, 39, 57] electrodes. In addition, the highest FoM value measured for our printed Ag NWs electrodes exceeds 1100, further demonstrating the superiority over other transparent conductor technologies, such as Ag grids[22], Ag nanothrough[50], Ag fiber[1], metal mesh[32], copper (Cu) NWs[17], gold (Au) mesh[21] and commercial indium tin oxide[8]. Only a handful of studies on Ag nanofiber[43], Cu nanotrough[50] and Cu veins[59], reported higher FoM than our printed Ag NWs films. However, our method allows for direct, high throughput printing of Ag NWs electrodes of arbitrary shape over a large area, temperature-sensitive substrates.

After the FLS, the electrical conductivity (σ) of the Ag NW patterns has been calculated based on the measured resistance (R) and the line geometries (i.e., line width [w], line length [l], line thickness [t]), following the Equation: $\sigma = l/(Rwt)$. As illustrated in Fig. 3a, the measured resistance per unit length decreases sharply when the printed line width increases from 50 μm to 300 μm, followed by a less pronounced drop for line widths >300 μm. This is because that some Ag NWs did not pass through the opening mesh to form lines with a width of about 50 μm due to the smaller size of the actual opening mesh (less than 38 μm) than the Ag NWs (20-60 μm). When the line width increases, the amount of Ag NWs transferred to the substrates increases, consequently leading to the formation of thicker electrodes. The thickness of the Ag NW electrodes is found to increase from 106 to 206 nm as the line width increased from 50 μm to 300 μm, followed by a smaller increase for line widths in the range of 300 to 500 μm (Fig. 3b). The result is consistent with the calculated conductivity of the printed lines, where the conductivity increases from 2.1×10^6 to 5.5×10^6 S/m as the line width increases from 50 to 500 μm (Fig. 3c). The calculated conductivity of our screen-printed, flash-sintered Ag NW electrodes is highly competitive to values found in the literature Ag NW electrodes processed via different methods[19, 37].

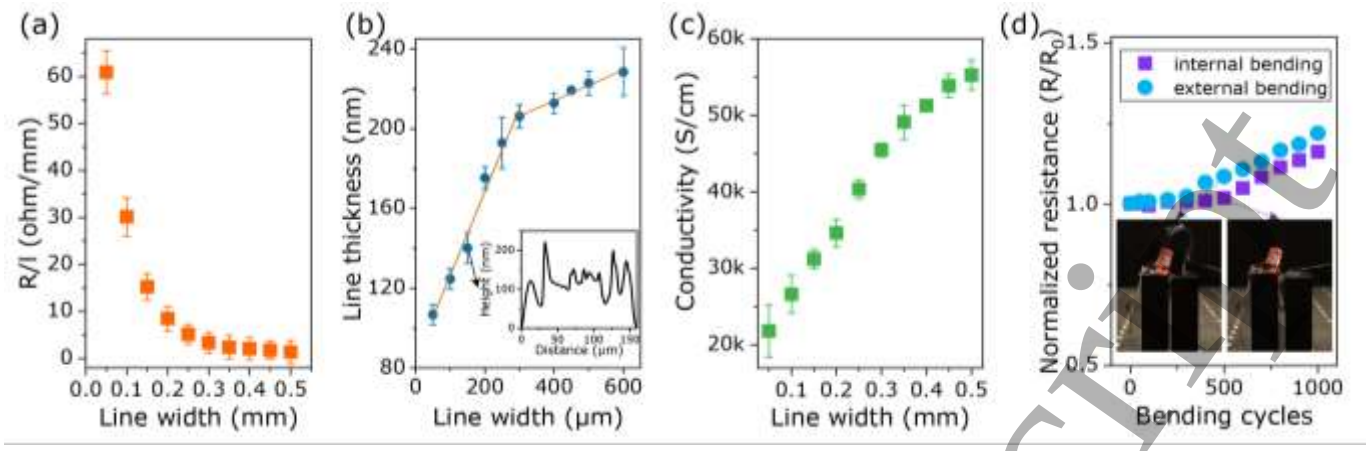

Fig. 3. (a) Resistance per unit length of the Ag NW lines as a function of line width. (b) Line thickness of the Ag NW lines as a function of line width. The orange line is a fitting curve. Inset is profile height of a printed Ag NW line with a width of 150 μm. (c) The calculated conductivity of the printed and sintered Ag NW patterns as a function of line width from 0.05 mm to 0.5 mm. (d) Normalized resistance change of Ag NW lines under cyclic bending. Insets are LED light connected to the Ag NW line.

In addition to the outstanding electrical and optical characteristics, mechanical stability is also important factor for practical applications in flexible and transparent electronics. To investigate the reliability of the screen-printed Ag NWs patterns under mechanical stress, resistance changes of the Ag NWs are monitored during bending both in internal (compressing) and external (extending) conditions. Fig. 3d shows that after continuous bending for over 1000 cycles, the resistance of the Ag NW electrodes with a width of 0.5 mm and length of 5 mm only increases by 16% and 22% for internal and external bending, respectively. Despite this increase, the test circuit maintains its conductivity to light a LED (inset of Fig. 3d), without evidence for any catastrophic failure/fracture during bending cycles.

The high optical transparency, excellent electrical conductivity, and outstanding mechanical stability make our Ag NW electrodes ideal for application in various electronic devices. To demonstrate the potential of the technology, we apply the screen-printed, flash-sintered Ag NW electrodes in RF field. In particular, we design and characterize a flexible, transparent fractal antenna for Wi-Fi (2.4 GHz), Bluetooth (2.4 GHz), and low-band 5G (3.5-4.2 GHz) applications. Fig. S8 provides the detailed geometric dimensions and 3D

model of the antenna in the full-wave electromagnetic simulation software and one photo of fabricated antenna. The minimum line length and the gap of the design are 0.4 and 0.15 mm, respectively. Both the antenna layer and the ground layer are made of screen-printed and flash-sintered Ag NWs with sharp and clear edges (magnified SEM images in Fig. 4a), demonstrating the reliability and high-resolution of our screen-printing process.

To quantitatively evaluate the antenna performance, we first study the antenna's reflection coefficient (S_{11}), which represents the ratio of the reflected electromagnetic wave to the incident electromagnetic wave for a certain frequency range. The frequency range at which the antenna has low S_{11} (below -10 dB), where less than 10% of power is reflected back, is considered the impedance bandwidth of the antenna. As presented in Fig. 4b, the measured S_{11} of the printed antenna matches the simulated results, with acceptable discrepancies. In particular, two reflection peaks at the frequencies of 2.3 and 4.1 GHz have been observed in the measurement, which is close to the simulated values of 2.3 and 4.3 GHz. The impedance bandwidth are 3.3 GHz (from 1.5 to 4.8 GHz) and 2.1 GHz (from 1.9 to 3.1 GHz and from 3.8 to 4.7 GHz) for the measured and simulated results, respectively, which cover the wireless standards, such as Wi-Fi, Bluetooth, and low-band 5G. The antenna's radiation properties, including antenna gain and radiation pattern are measured in a nearfield anechoic chamber (Star Lab from Satimo) and are depicted, along with the simulated results, in Fig. 4c and Fig. S9a. Again, the trend between the simulation and measured curves is similar. The differences between the measured and simulated results can be attributed to the under-estimation of conductive and dielectric losses in simulations and the rough surface of the printed Ag NW film. Nonetheless, the antenna demonstrates a decent impedance bandwidth and a gain of above 1 dBi for the frequency range of 2.3 to 4.1 GHz. Furthermore, the antenna has a decent omnidirectional radiation pattern, as expected for a monopole antenna. The E- and H-planes of the antenna radiation patterns are displayed in Fig. S9a at 2.4 GHz. Overall, the performance of this low-cost printed transparent antenna is comparable to standard printed circuit board-based antennas.

The flexibility and reliability of the Ag NW antenna under mechanical deformations is also studied. Despite the extreme bending conditions, with a bending radius of 10 mm, no measurable change in the bandwidth is observed even after 100 bending cycles (Fig. 4d). We also investigate the optical transparency of the Ag NW antenna by examining the transmittance over the entire visible wavelength (360 nm to 800 nm). The Ag NW antenna exhibits high optical transparency as displayed in the optical image in Fig. S9b, where the IMPACT logo can be clearly seen through the Ag NW antenna. The Ag NW antenna demonstrates a high transmittance of 87% at a wavelength of 550 nm, which is better than the previously reported optically transparent antennas in the literature, including metal nanoparticles (75%)[34], metal mesh (84.5%)[28], Ag coated polyester (80%)[41], conductive oxide (80%)[56], and graphene (85%)[13]. To demonstrate the scalability of the process, Fig. 4e presents five printed Ag NW antennas, which are prepared under the same printing parameters, sintering process, and sealing condition. All the antennas demonstrate similar RF performance (Fig. 4f), validating the scalability, repeatability, and reliability of our fabrication procedures.

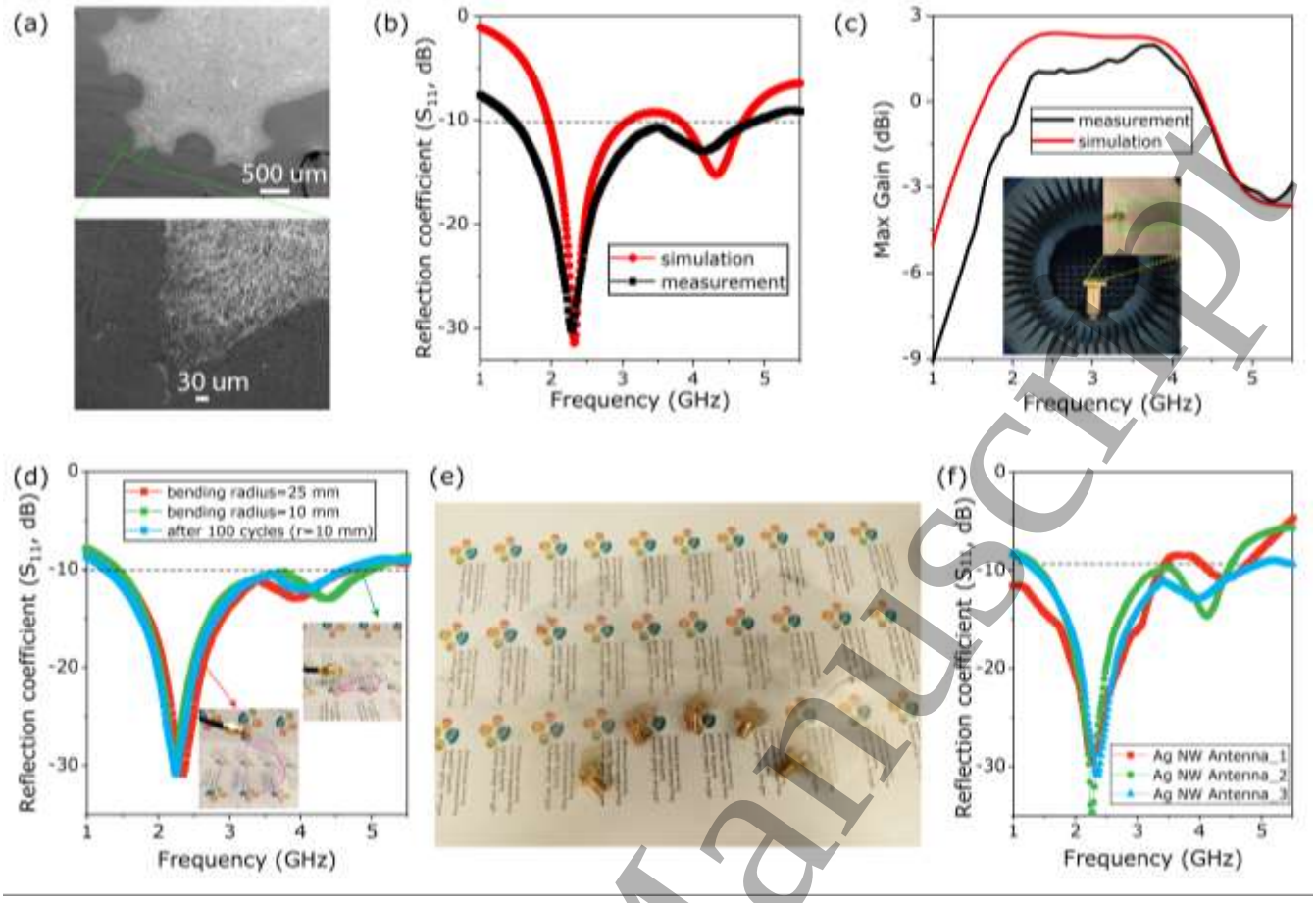

Fig. 4. RF performance of the printed Ag NW antenna: (a) SEM images of the printed Ag NW antenna (bottom panel displays the fine features of the antenna); (b) the measured and simulated return loss of the Ag NW antenna; (c) the measured and simulated antenna gain in the frequency of 1 to 5.5 GHz (inset is an Ag NW antenna under test in an anechoic chamber); (d) the measured S_{11} of the Ag NW antenna under mechanical deformation with different bending radius and cyclic bending at a bending radii of 10 mm (insets: digital photographs of the Ag NW antenna under bending conditions); (e) digital photograph and (f) the measured S_{11} of three Ag NW antennas.

Conclusions

In summary, screen-printable Ag NW ink with Ag NW loading as low as 0.9 wt% is developed via dispersing Ag NWs into a highly viscous PVP matrix. With the ink, Ag NW patterns with a large area (200 × 200 mm^2), high efficiency (up to 200 mm/s), high resolution (line width of about 50 μm), high optical transparency (92.2% transmittance at λ = 550 nm), high electrical conductivity (larger than 2×10^6 S/m),

and high FoM (more than 1100) are obtained via screen-printing and FLS. The additive manufacturing nature of screen-printing makes our Ag NW electrode technology for the mass production of flexible and transparent electronic devices. A fractal Ag NW-based antenna demonstrates well-matched RF performance with simulations, including return loss, antenna gain, and radiation pattern. The fully-printed Ag NW antennas exhibit remarkable mechanical stability under continuous bending (100 cyclic bending with a radius down to 10 mm) and high optical transparency (transmittance of 87% at λ = 550 nm). The combination of remarkable electrical, optical, and mechanical properties makes the screen-printed Ag NW electrodes a much promising technology for application in flexible, large-area, transparent electronics and RF components.

Conflicts of interest

There are no conflicts to declare.

Acknowledgements

The research for this paper is financially supported by King Abdullah University of Science and Technology (KAUST).

References

[1] Bai X, Lin S, Wang H, Zong Y, Wang H, Huang Z, Li D, Wang C and Wu H 2018 Room-temperature processing of silver submicron fiber mesh for flexible electronics *npj Flexible Electronics* **2** 3

[2] Cai L, Zhang S, Zhang Y, Li J, Miao J, Wang Q, Yu Z and Wang C 2017 Direct Printing for Additive Patterning of Silver Nanowires for Stretchable Sensor and Display Applications *Advanced Materials Technologies*

[3] Chen S, Guan Y, Li Y, Yan X, Ni H and Li L 2017 A water-based silver nanowire ink for large-scale flexible transparent conductive films and touch screens *J. Mater. Chem. C* **5** 2404-14

[4] Cho S, Kang S, Pandya A, Shanker R, Khan Z, Lee Y, Park J, Craig S L and Ko H 2017 Large-Area Cross-Aligned Silver Nanowire Electrodes for Flexible, Transparent, and Force-Sensitive Mechanochromic Touch Screens *ACS Nano* **11** 4346-57

[5] Chou N, Kim Y and Kim S 2016 A Method to Pattern Silver Nanowires Directly on Wafer-Scale PDMS Substrate and Its Applications *ACS Appl. Mater. Interfaces* **8** 6269-76

[6] Chung W-H, Park S-H, Joo S-J and Kim H-S 2018 UV-assisted flash light welding process to fabricate silver nanowire/graphene on a PET substrate for transparent electrodes *Nano Res.* **11** 2190-203

[7] Cui F, Yu Y, Dou L, Sun J, Yang Q, Schildknecht C, Schierle-Arndt K and Yang P 2015 Synthesis of Ultrathin Copper Nanowires Using Tris(trimethylsilyl)silane for High-Performance and Low-Haze Transparent Conductors *Nano Lett.* **15** 7610-5

[8] De S, Higgins T M, Lyons P E, Doherty E M, Nirmalraj P N, Blau W J, Boland J J and Coleman J N 2009 Silver Nanowire Networks as Flexible, Transparent, Conducting Films: Extremely High DC to Optical Conductivity Ratios *ACS Nano* **3** 1767-74

[9] Ellmer K 2012 Past achievements and future challenges in the development of optically transparent electrodes *Nat. Photonics* **6** 809-17

[10] Finn D J, Lotya M and Coleman J N 2015 Inkjet printing of silver nanowire networks *ACS Appl. Mater. Interfaces* **7** 9254-61

[11] Garnett E C, Cai W, Cha J J, Mahmood F, Connor S T, Greyson Christoforo M, Cui Y, McGehee M D and Brongersma M L 2012 Self-limited plasmonic welding of silver nanowire junctions *Nat. Mater.* **11** 241-9

[12] Ge Y, Duan X, Zhang M, Mei L, Hu J, Hu W and Duan X 2018 Direct Room Temperature Welding and Chemical Protection of Silver Nanowire Thin Films for High Performance Transparent Conductors *J. Am. Chem. Soc.* **140** 193-9

[13] Grande M, Bianco G V, Laneve D, Capezzuto P, Petruzzelli V, Scalora M, Prudenzano F, Bruno G and D'Orazio A 2018 Optically transparent wideband CVD graphene-based microwave antennas *Appl. Phys. Lett.* **112** 251103

[14] Hoeng F, Denneulin A, Reverdy-Bruas N, Krosnicki G and Bras J 2017 Rheology of cellulose nanofibrils/silver nanowires suspension for the production of transparent and conductive electrodes by screen printing *Appl. Surf. Sci.* **394** 160-8

[15] Hong S, Lee H, Lee J, Kwon J, Han S, Suh Y D, Cho H, Shin J, Yeo J and Ko S H 2015 Highly stretchable and transparent metal nanowire heater for wearable electronics applications *Adv. Mater.* **27** 4744-51

[16] Hong S, Yeo J, Kim G, Kim D, Lee H, Kwon J, Lee H, Lee P and Ko S H 2013 Nonvacuum, Maskless Fabrication of a Flexible Metal Grid Transparent Conductor by Low-Temperature Selective Laser Sintering of Nanoparticle Ink *ACS Nano* **7** 5024-31

[17] Hsu P-C, Kong D, Wang S, Wang H, Welch A J, Wu H and Cui Y 2014 Electrolessly Deposited Electrospun Metal Nanowire Transparent Electrodes *Journal of the American Chemical Society* **136** 10593-6

[18] Huang Q, Al-Milaji K N and Zhao H 2018 Inkjet Printing of Silver Nanowires for Stretchable Heaters *ACS Applied Nano Materials* **1** 4528-36

[19] Huang Q and Zhu Y 2018 Gravure Printing of Water-based Silver Nanowire ink on Plastic Substrate for Flexible Electronics *Sci. Rep.* **8** 15167

[20] Hyun W J, Secor E B, Hersam M C, Frisbie C D and Francis L F 2015 High-Resolution Patterning of Graphene by Screen Printing with a Silicon Stencil for Highly Flexible Printed Electronics *Adv. Mater.* **27** 109-15

[21] Jang S, Jung W-B, Kim C, Won P, Lee S-G, Cho K M, Jin M L, An C J, Jeon H-J, Ko S H, Kim T-S and Jung H-T 2016 A three-dimensional metal grid mesh as a practical alternative to ITO *Nanoscale* **8** 14257-63

[22] Jang Y, Kim J and Byun D 2013 Invisible metal-grid transparent electrode prepared by electrohydrodynamic (EHD) jet printing *J. Phys. D: Appl. Phys.* **46** 155103

[23] Jeon I, Yoon J, Kim U, Lee C, Xiang R, Shawky A, Xi J, Byeon J, Lee H M, Choi M, Maruyama S and Matsuo Y 2019 High-Performance Solution-Processed Double-Walled Carbon Nanotube Transparent Electrode for Perovskite Solar Cells **9** 1901204

[24] Jin Y, Li L, Cheng Y, Kong L, Pei Q and Xiao F 2015 Cohesively Enhanced Conductivity and Adhesion of Flexible Silver Nanowire Networks by Biocompatible Polymer Sol-Gel Transition *Adv. Funct. Mater.* **25** 1581-7

[25] Jung J, Lee H, Ha I, Cho H, Kim K K, Kwon J, Won P, Hong S and Ko S H 2017 Highly Stretchable and Transparent Electromagnetic Interference Shielding Film Based on Silver Nanowire Percolation Network for Wearable Electronics Applications *ACS Appl. Mater. Interfaces* **9** 44609-16

[26] Kang S, Kim T, Cho S, Lee Y, Choe A, Walker B, Ko S-J, Kim J Y and Ko H 2015 Capillary Printing of Highly Aligned Silver Nanowire Transparent Electrodes for High-Performance Optoelectronic Devices *Nano Lett.* **15** 7933-42

[27] Ko Y, Kim J, Kim D, Yamauchi Y, Kim J H and You J 2017 A Simple Silver Nanowire Patterning Method Based on Poly(Ethylene Glycol) Photolithography and Its Application for Soft Electronics *Sci. Rep.* **7** 2282

[28] Kubwimana J L, Kirsch N J, Ziegler C, Kontopidis G and Tuner B 2019 Dual-Polarized 5.75 GHz Optically Transparent Antenna Arrays *IEEE Antennas Wirel. Propag. Lett.* **18** 1512-6

[29] Lee C, Oh Y, Yoon I S, Kim S H, Ju B-K and Hong J-M 2018 Flash-induced nanowelding of silver nanowire networks for transparent stretchable electrochromic devices *Sci. Rep.* **8** 2763

[30] Lee H B, Jin W-Y, Ovhal M M, Kumar N and Kang J-W 2019 Flexible transparent conducting electrodes based on metal meshes for organic optoelectronic device applications: a review *J. Mater. Chem. C* **7** 1087-110

[31] Lee M-S, Lee K, Kim S-Y, Lee H, Park J, Choi K-H, Kim H-K, Kim D-G, Lee D-Y, Nam S and Park J-U 2013 High-Performance, Transparent, and Stretchable Electrodes Using Graphene–Metal Nanowire Hybrid Structures *Nano Lett.* **13** 2814-21

[32] Lee S M, Oh S and Chang S T 2019 Highly Transparent, Flexible Conductors and Heaters Based on Metal Nanomesh Structures Manufactured Using an All-Water-Based Solution Process *ACS Appl. Mater. Interfaces* **11** 4541-50

[33] Li B, Ye S, Stewart I E, Alvarez S and Wiley B J 2015 Synthesis and Purification of Silver Nanowires To Make Conducting Films with a Transmittance of 99% *Nano Lett.* **15** 6722-6

[34] Li Q L, Cheung S W, Wu D and Yuk T I 2017 Optically Transparent Dual-Band MIMO Antenna Using Micro-Metal Mesh Conductive Film for WLAN System *IEEE Antennas Wirel. Propag. Lett.* **16** 920-3

[35] Li W, Yang S and Shamim A 2019 Screen printing of silver nanowires: balancing conductivity with transparency while maintaining flexibility and stretchability *npj Flexible Electronics* **3** 13

[36] Liang J, Li L, Tong K, Ren Z, Hu W, Niu X, Chen Y and Pei Q 2014 Silver Nanowire Percolation Network Soldered with Graphene Oxide at Room Temperature and Its Application for Fully Stretchable Polymer Light-Emitting Diodes *ACS Nano* **8** 1590-600

[37] Liang J, Tong K and Pei Q 2016 A Water-Based Silver-Nanowire Screen-Print Ink for the Fabrication of Stretchable Conductors and Wearable Thin-Film Transistors *Adv. Mater.* **28** 5986-96

[38] Liu G S, Liu C, Chen H J, Cao W, Qiu J S, Shieh H P and Yang B R 2016 Electrically robust silver nanowire patterns transferrable onto various substrates *Nanoscale* **8** 5507-15

[39] Liu J-W, Wang J-L, Wang Z-H, Huang W-R and Yu S-H 2014 Manipulating Nanowire Assembly for Flexible Transparent Electrodes *Angew. Chem. Int. Ed.* **53** 13477-82
[40] Liu Y, Zhang J, Gao H, Wang Y, Liu Q, Huang S, Guo C F and Ren Z 2017 Capillary-Force-Induced Cold Welding in Silver-Nanowire-Based Flexible Transparent Electrodes *Nano Lett.* **17** 1090-6
[41] Malek M A, Hakimi S, Rahim S K A and Evizal A K 2015 Dual-Band CPW-Fed Transparent Antenna for Active RFID Tags *IEEE Antennas Wirel. Propag. Lett.* **14** 919-22
[42] Ning J, Hao L, Jin M, Qiu X, Shen Y, Liang J, Zhang X, Wang B, Li X and Zhi L 2017 A Facile Reduction Method for Roll-to-Roll Production of High Performance Graphene-Based Transparent Conductive Films *Adv. Mater.* **29**
[43] Park J, Hyun B G, An B W, Im H-G, Park Y-G, Jang J, Park J-U and Bae B-S 2017 Flexible Transparent Conductive Films with High Performance and Reliability Using Hybrid Structures of Continuous Metal Nanofiber Networks for Flexible Optoelectronics *ACS Appl. Mater. Interfaces* **9** 20299-305
[44] Park J H, Hwang G T, Kim S, Seo J, Park H J, Yu K, Kim T S and Lee K J 2017 Flash-Induced Self-Limited Plasmonic Welding of Silver Nanowire Network for Transparent Flexible Energy Harvester *Adv. Mater.* **29**
[45] Ricciardulli A G, Yang S, Wetzelaer G-J A H, Feng X and Blom P W M 2018 Hybrid Silver Nanowire and Graphene-Based Solution-Processed Transparent Electrode for Organic Optoelectronics *Adv. Funct. Mater.* **28**
[46] Teymouri A, Pillai S, Ouyang Z, Hao X, Liu F, Yan C and Green M A 2017 Low-Temperature Solution Processed Random Silver Nanowire as a Promising Replacement for Indium Tin Oxide *ACS Appl. Mater. Interfaces* **9** 34093-100
[47] Tokuno T, Nogi M, Karakawa M, Jiu J, Nge T T, Aso Y and Suganuma K 2011 Fabrication of silver nanowire transparent electrodes at room temperature *Nano Res.* **4** 1215-22
[48] Trung T N, Kim D O, Lee J H, Dao V D, Choi H S and Kim E T 2017 Simple and Reliable Lift-Off Patterning Approach for Graphene and Graphene-Ag Nanowire Hybrid Films *ACS Appl. Mater. Interfaces* **9** 21406-12
[49] Wang J, Liang M, Fang Y, Qiu T, Zhang J and Zhi L 2012 Rod-coating: towards large-area fabrication of uniform reduced graphene oxide films for flexible touch screens *Adv. Mater.* **24** 2874-8
[50] Wu H, Kong D, Ruan Z, Hsu P C, Wang S, Yu Z, Carney T J, Hu L, Fan S and Cui Y 2013 A transparent electrode based on a metal nanotrough network *Nat. Nanotechnol.* **8** 421-5
[51] Wu J, Que X, Hu Q, Luo D, Liu T, Liu F, Russell T P, Zhu R and Gong Q 2016 Multi-Length Scaled Silver Nanowire Grid for Application in Efficient Organic Solar Cells *Adv. Funct. Mater.* **26** 4822-8
[52] Xiong J, Li S, Ye Y, Wang J, Qian K, Cui P, Gao D, Lin M F, Chen T and Lee P S 2018 A Deformable and Highly Robust Ethyl Cellulose Transparent Conductor with a Scalable Silver Nanowires Bundle Micromesh *Adv. Mater.* e1802803
[53] Xu F, Xu W, Mao B, Shen W, Yu Y, Tan R and Song W 2018 Preparation and cold welding of silver nanowire based transparent electrodes with optical transmittances >90% and sheet resistances <10 ohm/sq *J. Colloid Interface Sci.* **512** 208-18
[54] Yang J, Bao C, Zhu K, Yu T and Xu Q 2018 High-Performance Transparent Conducting Metal Network Electrodes for Perovksite Photodetectors *ACS Appl. Mater. Interfaces* **10** 1996-2003
[55] Yao S and Zhu Y 2014 Wearable multifunctional sensors using printed stretchable conductors made of silver nanowires *Nanoscale* **6** 2345-52
[56] Yao Y, Chen W, Chen X and Yu J 2017 Design of Optically Transparent Antenna with Directional Radiation Patterns *International Journal of Antennas and Propagation* **2017** 7
[57] Yim J H, Joe S-y, Pang C, Lee K M, Jeong H, Park J-Y, Ahn Y H, de Mello J C and Lee S 2014 Fully Solution-Processed Semitransparent Organic Solar Cells with a Silver Nanowire Cathode and a Conducting Polymer Anode *ACS Nano* **8** 2857-63
[58] Yoo B, Kim Y, Han C J, Oh M S and Kim J-W 2018 Recyclable patterning of silver nanowire percolated network for fabrication of flexible transparent electrode *Appl. Surf. Sci.* **429** 151-7
[59] Yu Y, Zhang Y, Li K, Yan C and Zheng Z 2015 Bio-Inspired Chemical Fabrication of Stretchable Transparent Electrodes *Small* **11** 3444-9
[60] Zeng X Y, Zhang Q K, Yu R M and Lu C Z 2010 A new transparent conductor: silver nanowire film buried at the surface of a transparent polymer *Adv. Mater.* **22** 4484-8
[61] Zhao P, Tang Q, Zhao X, Tong Y and Liu Y 2018 Highly stable and flexible transparent conductive polymer electrode patterns for large-scale organic transistors *J. Colloid Interface Sci.* **520** 58-63